ARTICLE

In vitro Immunogenicity of Silicon-Based Micro- and Nanostructured Surfaces

Kristy M. Ainslie,[†,∥] Sarah L. Tao,[†,‡] Ketul C. Popat,[†,§] and Tejal A. Desai[†,∥,*]

[†]Department of Bioengineering and Therapeutic Sciences, and [∥]Department of Physiology, University of California, San Francisco, San Francisco, California 94158, [‡]The Charles Stark Draper Laboratory, Cambridge, Massachusetts 02139, and [§]Department of Mechanical Engineering/School of Biomedical Engineering, Colorado State University, Fort Collins, Colorado 80523

ABSTRACT The increasing use of micro- and nanostructured silicon-based devices for *in vivo* therapeutic or sensing applications highlights the importance of understanding the immunogenicity of these surfaces. Four silicon surfaces (nanoporous, microstructured, nanochanneled, and flat) were studied for their ability to provoke an immune response in human blood derived monocytes. The monocytes were incubated with the surfaces for 48 h and the immunogenicity was evaluated based on the viability, shape factors, and cytokine expression. Free radical oxygen formation was measured at 18 h to elicit a possible mechanism invoking immunogenicity. Although no cytokines were significantly different comparing the response of monocytes on the tissue culture polystyrene surfaces to those on the micropeaked surfaces, on average all cytokines were elevated on the micropeaked surface. The monocytes on the nanoporous surface also displayed an elevated cytokine response, overall, but not to the degree of those on the micropeaked surface. The nanochanneled surface response was similar to that of flat silicon. Overall, the immunogenicity and biocompatibility of flat, nanochanneled, and nanoporous silicon toward human monocytes are approximately equivalent to tissue culture polystyrene.

KEYWORDS: nanoporous silicon · nanostructured silicon · inflammation · inflammatory response · microstructured silicon · human monocytes

The application of micro- and nanotechnology to the biomedical arena has tremendous potential in terms of developing new therapeutic modalities. Microelectronic process engineering was a discipline that developed owing to the rapid growth of the integrated circuit industry. Traditionally, microelectromechanical systems (MEMS) research has been used to produce functional devices on the micrometer scale, such as sensors, switches, filters, and gears, from silicon, the dominant material used throughout the IC industry. These devices are fabricated by the repeated application of unit process steps such as thin-film deposition, photolithography, and etching, which allow for the precise control over micro-/nanoarchitecture. Many silicon-based devices, such as implantable sensors[1,2] and devices for drug delivery,[3–5] as well as electrical stimulation,[6–8] are already in consideration for use within the human body. There are other numerous examples of MEMS-based biomedical devices.[9–18] Silicon itself is not typically regarded as a biomaterial that could directly interface with living tissue; therefore these implants and their circuitry are usually completely isolated from the body utilizing other materials for packaging such as a titanium, polymers, or ceramics.

With the development of such novel micromachined systems, it has become increasingly important to both understand and control responses at the biological interface of these devices. To achieve such control, biomaterials can be topographically modified at their surface in order to modulate biological interaction. Micro- and nanostructured silicon, such as porous and nanowired silicon, has previously been employed as a foundation for sensor technology.[19–27] It has been shown that topographically modified silicon can illicit specific physiological responses within the body, from bioactivity[28–31] to biodegradation.[32–36] These material properties can potentially be exploited for numerous medical applications including tissue engineering,[37–42] and drug delivery.[3,43–46]

Studies have been performed on the biocompatibility, biofouling, and tissue reactions to silicon-based material,[47–50] as well as topographically modified nano- and microstructured silicon.[51–57] However, relatively little is known about the immunogenicity of these materials. Traditionally, biocompatibility refers to the performance of a material in the appropriate realm for a given application,[58] usually by testing the viability of one or more cells or tissues in contact with the surface. In contrast, immunogenicity of a material encompasses not only the response of immune cells to the surface, but also the cellular signals released that may

*Address correspondence to Tejal.desai@ucsf.edu.

Received for review February 4, 2008 and accepted April 24, 2008.

Published online May 27, 2008.
10.1021/nn800071k CCC: $40.75

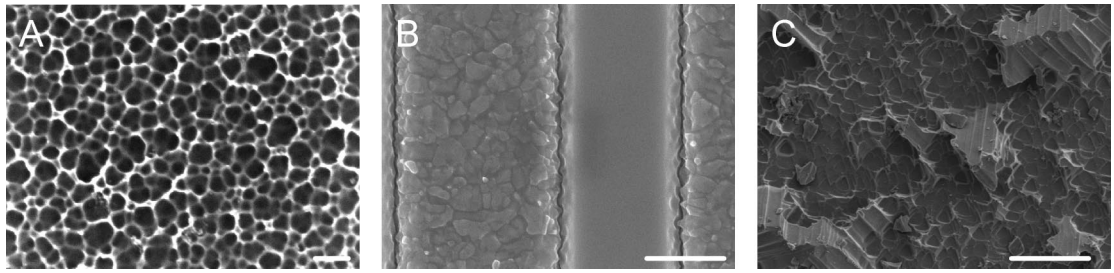

Figure 1. Scanning electron images of structured silicon surfaces: (A) nanoporous Si, scale bar = 200 nm; (B) nanochanneled Si, scale bar = 1 μm; (C) micropeaked silicon, scale bar = 10 μm.

initiate immune cell migration and encapsulation, or inflammation. A small number of studies have been performed with immune cells on silicon surfaces or silane-modified surfaces,[59,60] as well as the toxicity and inflammatory response toward silicon nanoparticles.[61] However, no extensive research has been performed on the immunogenicity of micro- and nanostructured silicon surfaces. Ultimately, understanding the immunogenicity and inflammation response of bulk, micromachined, and topographically modified silicon will help in discerning how implanted silicon-based devices can be optimized to elicit a desired biological response.

In this study human blood-derived monocytes were seeded on nanoporous, micropeaked, nanochanneled and flat silicon (Figure 1). Primary monocytes were chosen because of their well-characterized cytokine expression. Immortalized macrophage cell lines (*e.g.*, RAW) have also been characterized in literature; however their expression levels differ from primary derived monocytes[62] and in the field of immunology it is commonplace to use primary derived cells. Live/dead ratios, cell shape factors, and a 10 panel cytokine profile (IL-1α and β, IL-12, IL-6, TNF-α, IFN-α and γ, MIP-1α and β, and anti-inflammatory IL-10 and IL-6) were integrated to determine the immunogenicity of the bulk, micromachined, and topographically modified silicon surfaces. Reactive oxygen and superoxide species were monitored in monocytes on the silicon surfaces to explore a possible mechanism for surface immunogenicity. A definition of these cytokines and free-radical species is given in Table 1.

RESULTS AND DISCUSSION

Cell Viability and Morphology on Silicon Surfaces. Evaluating cell viability is important for the application of silicon-based biomedical devices *in vivo*. High amounts of non-regulated cell death, in conjunction with a foreign material, can lead to a heightened inflammation response, resulting in a broad chronic inflammation and perhaps a nonspecific systemic attack of other cells and tissues.[63–66] The percent of live cells is given in Figure 2. The highest percent of live cells is on the flat silicon with the nanochanneled silicon only a fraction lower, 97.4 ± 6.0% and 89.8 ± 16.4%, respectively. The per-

TABLE 1. Cytokine Definitions for Inflammation Panel Results in Table 3.[63,64]

Cytokine Expression		
	description	**pro-inflammatory?**
IL-1α	Produced in response to cell injury to induce apoptosis.	yes
IL-1β	Involved in cell proliferation, differentiation and apoptosis.	yes
IL-6	Linked to an antiwound healing response through promotion of local inflammation including cellular activation and immune cell chemotaxis. Down regulates pro-inflammatory cytokines IL-1 and TNF-α.	sometimes
IL-10	Regulates pro-inflammatory cytokines like IFN-γ, IL-2, IL-3, TNF-α and GM-CSF but can be stimulatory toward T-cells, mast cells, and B cells.	sometimes
IFN-α	Traditionally expressed in response to viral infections.	yes
IFN-γ	Activates macrophage and natural killer lymphocytes.	yes
TNF-α	Causes apoptotic cell death, cellular proliferation, differentiation, and inflammation.	yes
IL-12	Stimulates the growth and function of T cells.	yes
MIP-1α	Promotes chemotaxis of immune cells, including macrophages.	yes
MIP-1β	Promote immune cell chemotaxis and induces the synthesis and release of other pro-inflammatory cytokines.	yes

Free-Radical Oxygen Species Formation		
acronym	**species detected**	**description**
ROS	hydrogen peroxide (H_2O_2), peroxy radicals (ROO●), peroxynitrite (OONO-) oxides	Free radical oxygen ions formed through a variety of methods including UV activation, dissolution of material, hydro-phobic/phillic interactions, and red-ox cycling. Can overtake the cells natural antioxidant defense and lead to cellular inflammation and release of pro-inflammatory cytokines.
mitochondrial superoxide	mitochondrial superoxide anions (●O_2-)	Can be formed by incomplete cellular respiration during healthy cell activity. Serves as a sign of overwhelming ROS formation.

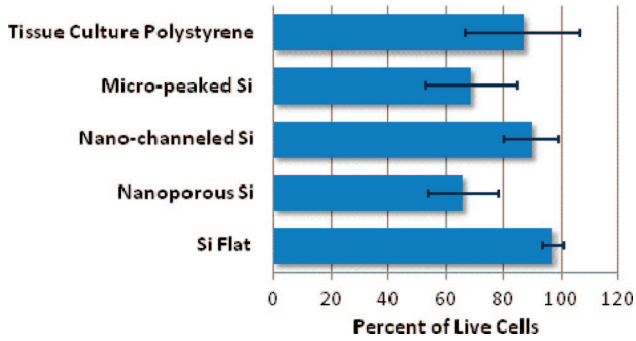

Figure 2. The percentage of live monocytes adherent to the surface of the micro- and nanomaterials. Adherent monocytes were stained with propidium iodide to indicate cell death and CellTracker Green CMFDA to indicate live cells. Cells were imaged after 48 h of culturing on the surface. Data is presented as average plus or minus standard error mean. Data is in the absence of statistical significance. Sample size, $n = 3$. Monocytes were derived from three or more blood donors of varying ethnic background.

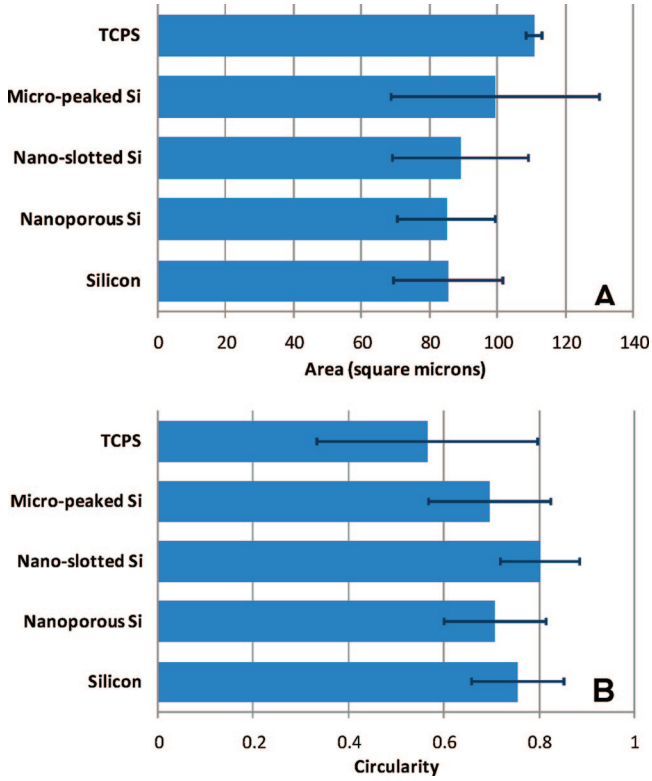

Figure 3. Area (A) and circularity (B) for adherent monocytes on nanomaterials. Area and circularity measurements were measured using ImageJ by manually tracing the cells outline as imaged fluorescently with CellTracker Green CMFDA. Cells were analyzed after 48 h of culturing on the surface. An increase in cell area and a decrease in cell circularity are indicative of monocyte activation or stimulation.[68] Data is presented as average plus or minus standard error mean. Data is in the absence of statistical significance. Sample size, $n = 3$. Monocytes were derived from three or more blood donors of varying ethnic background.

cent live cells on nanoporous and micropeaked silicon were both approximately 70%.

Cell area and circularity measurements are presented in Figure 3. Figure 3a represents the area of the cell in square micrometers and Figure 3b presents the nondimensional value of circularity. A circularity value

TABLE 2. Cytokines Released by Monocytes Incubated with Nanomaterial[a]

	IL-1α	IL-1β	TNF-α	IFN-α	IFN-γ
Si flat	52**	**<6****	**8****	39*	20**
nanoporous Si	56**	**30****	12**	39*	15**
nanochanneled Si	52**	41**	12**,S	54	16**
micropeaked Si	88	113**	33**	58	58*
LPS	**92**	**714**	160	**72**	**155**
TCPS	51	60	14	33	17
media	54	14	<3	38	<22

	IL-12	IL-10	IL-6	MIP-1α	MIP-1β
Si flat	148**	45**	**317****	65**	83**
nanoporous Si	187**	133**	**845***	**114****	157**
nanochanneled Si	156**	33**	69*,S,^	65**	121**,S
micropeaked Si	334**	187**	2,211*	380**	523**
LPS	**1374**	**4595**	**59100**	**16551**	**12722**
TCPS	134	26	69	57	116
media	12	14	2	10	<16

[a]Concentrations are presented in pictograms per milliliter. Significance is reported with respect to tissue culture polystyrene (**bold**), lipopolysaccharide (*), silicon (S), and nanoporous silicon (^). A single indication (*e.g.*, *) denotes a p-value < 0.05 and a double indication (*e.g.*, **) indicated p-value < 0.01. Sample size: $n = 3$. Monocytes were derived from four or more blood donors of varying ethnic background.

of one indicates the cell is a perfect circle. A value less than one indicates a noncircular or spread shape. On average, the monocytes are larger in area and less circular on the micropeaked surface than on the other surfaces, indicating the cells are more spread on the micropeaked surface.

Monocyte morphology is one of the earliest consequences of activation. Morphology can change under various types of stresses, including contact with material surfaces. Cell morphology was examined here using scanning electron microscopy. Images of monocytes on the material surface are presented in Figure 4: (A) Si flat, (B) nanoporous Si, (C) nanochanneled silicon, (D) micropeaked silicon, (E) LPS, and (F) tissue culture polystyrene (TCPS). The monocytes on all surfaces display, to an extent, morphology associated with monocyte activation. The activated cells have increased plane area, are more spread, and display migratory ruffles or pseudopodia associated with cytoplasmic spreading. One exception is the monocytes cultured on the micropeaked surface. Although these cells are larger in size and display increased ruffling of the membrane surface, they remain spherical in shape.

The cellular response to planar and nanoporous silicon has been studied in literature, though biocompatibility varies with cell type. Bayliss *et al.* concluded that planar silicon[53] and nanoporous silicon[52] are both biocompatible, for CHO and B50 cells, in terms of greater cellular adhesion,[52,67] and that the cells preferred growing on nanoporous silicon in comparison to control glass surfaces.[67] Porous silicon was also deemed bio-

TABLE 3. ROS Superoxides and Oxygen Free Radicals Mean Fluorescent Intensities Normalized with Respect to Tissue Culture Polystyrene (TCPS)[a]

	reactive oxygen species	superoxide species
Si flat	135 ± 29%	92 ± 4%
nanoporous Si	87 ± 8%	73 ± 2%
nanochanneled Si	104 ± 7%	71 ± 9%
micropeaked Si	4055 ± 1156% S*	37 ± 4%
LPS	272 ± 65%	164 ± 39%
TCPS	100 ± 56%	100 ± 3%

[a]Significance with respect to the flat silicon (S) and TCPS (*). Data is presented as average plus or minus standard error mean. Sample size: $n = 3$. Monocytes were derived from three or more blood donors of varying ethnic background.

compatible with hepatocytes, based on their protein release.[55] Here, findings indicate that monocytes react differently to silicon surfaces than other cell types. Cells with increased area and decreased circularity indicates activation or stimulation of the monocyte.[68] This is in contrast to traditional adherent cell studies where an increase in cell area is indicative of increased viability. On the basis of the area and circularity of monocytes micro- and nanostructured surfaces do not significantly promote an inflammation response *in vitro*.

Cytokine Release From of Monocytes on Silicon Surfaces. The summary of the cytokine analysis is presented in Table 2. All cytokine values are significantly different from the LPS positive control except IL-1α and IFN-α for the micropeaked silicon surface and IFN-α for the nanochanneled silicon. For nanochanneled silicon the amount of TNF-α and MIP-1β expressed by monocytes is significantly higher than those on the flat silicon surface, while IL-6 is significantly less than flat silicon. All expression levels for LPS, except TNF-α, are significantly higher than tissue culture polystyrene. For flat silicon, the values of IL-1β, and TNF-α are significantly lower, and those for IL-6 are significantly higher than those for TCPS. The values of expression for IL-1β is significantly lower, and those for IL-6 and MIP-1α are significantly higher than the expression on TCPS compared to nanoporous silicon.

The silicon micropeaked and nanoporous surfaces appear to be the most immunogenic of the four surfaces, with micropeaked silicon being the most immunostimulatory with high levels of IL-1, TNF-α, MIP-1, and IL-12. However, both surfaces had wide variation in their three sample results, resulting in broad standard deviations that were not larger than the sample average. Furthermore, it was found that cell viability is lowest and monocyte area is highest on the micropeaked surface.

For percent live, cytokine, and shape analysis, the nanochanneled silicon surface appears to be most similar to the flat silicon. The two cytokines that do not follow this trend are IL-6 and MIP-1β. IL-6 production is almost three times greater from monocytes on the flat silicon surface, and the MIP-1β concentration is significantly higher in the nanochanneled supernatant. IL-6 production is higher after monocytes adhere to the surface[69] and can possess chemotactic properties for various nonimmune cells types.[70] MIP-1β is a chemotactic for many inflammatory cells including T-cells, NK cells, macrophages, and monocytes.[71]

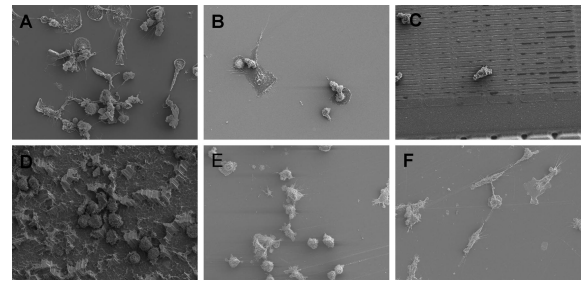

Figure 4. Scanning electron images of monocytes adhered to the biomaterial surface: (A) Si flat, (B) nanoporous Si, (C) nanochanneled Si, (D) micropeaked silicon, (E) LPS, and (F) TCPS. Scale bar = 20 μm. The activated cells have increased spreading and area. Often migratory ruffles or pseudopodia are displayed during activation. Monocytes were derived from three or more blood donors of varying ethnic background.

The previous studies involving silicon and inflammation or toxicity are focused on silicon-based nanoparticles,[72] bacteria,[73] plants,[74] or macrophage/monocyte giant cell formation on silicon or silane-modified surface.[59,60] Liao and Cui concluded that neuroinflammatory cytokine production was reduced with aptamer coating of the silicon surface.[75] The toxicity of neuroblastomas on silicon was correlated to the manufacturing process, rather than the material itself.[76] Indeed, residual silver on the surface of our micropeaked silicon after processing might also be a factor in the higher inflammation response observed with this surface. Silver has been shown to be severely cytotoxic.[77] In fact, X-ray photoelectron spectroscopy results (data not shown) indicate that micropeaked surfaces did possess some elemental impurities.

Despite the elevated inflammatory cytokines on especially the micropeaked surfaces, none of the surfaces are as inflammatory as the positive control lipopolysaccharide. The repeated saccharide structure of the bacterial-coated sugar causes receptor coupling on the monocyte surface, resulting in activation.[78] On the basis of the average expression of inflammatory cytokines, the LPS-stimulated monocytes are about 400% more inflamed than the monocytes on the micropeaked surface. The inflammatory cytokines released from monocytes on the negative control tissue culture polystyrene surface are roughly half the values of those expressed from monocytes on the micropeaked surface. Similarly, the LPS stimulated monocytes are approximately 950, 850, 750, and 850% more activated than the monocytes on the flat, nanochanneled, and nanoporous silicon and tissue culture polystyrene, respectively.

Relatively few studies have observed a panel of inflammatory cytokines in response to material micro- or

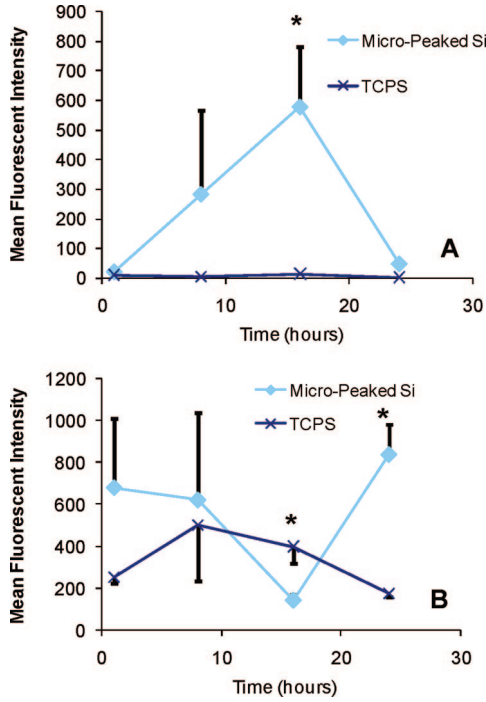

Figure 5. Time course of reactive oxygen species (a) and mitochondrial surperoxide (b) species in micropeaked silicon and tissue culture polystyrene surfaces. Reactive oxygen species can serve as an indicator of immunogenicity, wherein they overtake the cells antioxidant response leading to mitochondrial perturbations and superoxide formation. Data is presented as average, with the error bars denoting the value of standard error mean in either the positive or negative direction. An asterisk (*) denotes significance with respect to tissue culture polystyrene. Reactive oxygen species formation was measured through flow cytometry with fluorescent dye carboxy-H_2DCFDA. Mitochondrial superoxide expression was measured with MitoSOX red with flow cytometry. Sample size: $n = 3$. Monocytes were derived from three or more blood donors of varying ethnic background.

nanostructure. One such study observed that macrophages on nanofibrous polytetrafluoroethylene (nPTFE) show immunogenicity similar to tissue culture polystyrene, with no cytokines significantly elevated in the comparison.[79] It would appear that in contrast to high concentrations of nanoparticles[72] in contact with cells, micro- and nanostructured silicon surfaces are less likely to significantly stimulate the immune system.

Reactive Oxygen Species Formation of Monocytes on Silicon Surfaces. The time course of reactive oxygen species and mitochondrial superoxide are presented in Figure 5 panels a and b, respectively. All oxide species are presented as mean fluorescent intensities. The oxide species were monitored at the one, eight, sixteen, and twenty-four hour time points to determine the optimum time point for monitoring. The highest reactive oxygen species were detected at the sixteen hour time point, with the lowest mitochondrial superoxide concentration also at that point. At this time point, sixteen hours, all the other surfaces were evaluated (Table 3). Both the mitochondrial superoxide and reactive oxygen species are less on the nanoporous surface compared to the flat silicon surface. The micropeaked silicon surface displayed the greatest reactive oxygen species at this time point.

Reactive oxygen species formation has been indicated as a predictor of inflammation in macrophages cultured with nanoparticles.[72,80] Once the cell's antioxidant defense is overtaken with reactive oxygen species, the cell experiences oxidative stress and can release inflammatory or danger signals[81] to promote the migration of immune cells to the site of immunogenicity. Some of the common causes of reactive oxygen species formation are active electron configurations, UV activation leading to radical formation, dissolution of material, hydro-phobic/phillic interactions, and reduction−oxidation cycling.[72] In this study we observed four common types of reactive oxygen species. The reactive oxygen species detected with carboxy-H_2DCFDA were hydrogen peroxide (H_2O_2), peroxy radicals (ROO●), and peroxynitrite (OONO-) oxides. Mitochondrial superoxide anions (●O_2-) were monitored with the mitoSOX dye. Mitochondrial superoxides are usually formed during normal cellular respiration at a frequency of about 1−3% (Invitrogen). A high amount of mitochondrial oxidative species can indicate loss of mitochondrial potential[82] or an overwhelming of the cells antioxidant defense by ROS species.[83] Low amounts of reactive oxygen species can promote cell proliferation. High amounts can be cytotoxic and in fact immune cells use superoxide, and nitric oxide's reactive product peroxynitrite, to attack and kill invaders.[64] Additionally, reactive oxygen species can be used to degrade material surfaces.[66]

For the flat, nanoporous, and nanochanneled silicon, the reactive oxygen species is relatively low and does not follow the same trend with regard to expression of elevated inflammatory cytokines as do nanoparticles. Additionally, the number of dead cells on the surfaces does not seem to be linked to reactive oxygen species. The nonstatistically significant changes in area of the cell from surface to surface seem to be the only measured parameter that follows the same trend as the reactive oxygen species. Monocytes on all four surfaces seem to be minimally affected by the formation of mitochondrial superoxides, since all values are lower than on the negative control, tissue culture polystyrene. This seems to imply that although reactive oxygen species are present, they are not overwhelming enough to lead to mitochondrial perturbation.[83] The reactive oxygen species appear to be greatly affected by the micropeaked surface. The reactive oxygen normalized mean fluorescent intensity is elevated on the micropeaked surface. It appears that reactive oxygen species formation on micro- and nanostructured bulk materials is not necessarily a prerequisite for inflammation as proposed for nanoparticles.[72]

The ultimate goal in bioengineering the material interface of an implant is to make the device less sus-

ceptible to the host foreign body response and thus, failure. The foreign body response is characterized by protein adhesion and cellular adherence, resulting in a mass transfer barrier on the order of 10 to 100 μm over the course of 30 days or less.[66] Nanomaterials have been implicated as one of the many ways to reduce the foreign body response.[84,85] A common component of this response is the presence, adherence, and response of monocytes at the material surface. In this study it has been shown that the immunogenicity and biocompatibility of flat, nanochanneled and nanoporous silicon toward human monocytes are approximately equivalent to tissue culture polystyrene. The micropeaked surface is more immunogenic than all of the other evaluated surfaces. Also, the formation of reactive oxygen species is not a perquisite for inflammation in silicon-based surfaces.

METHODS

All chemicals were purchased from Sigma (St. Louis, MO) except where indicated.

Surface Preparation. ***Flat Silicon.*** Three inch p-type <100>, front-side polished, back-side etched, wafers were purchased from Addison Engineering (San Jose, Ca). Wafers were diced into 1 cm × 1 cm squares for experimental use or for further processing.

Nanoporous. Nanoporous silicon was formed by electrochemical anodization as previously described by Foraker *et al.*[86] A custom-made polypropylene anodization tank was filled with 50 mL of 49.7% hydrofluoric acid (HF) and 100% ethanol (1:1 by volume). Please note that HF is extremely dangerous and can cause severe burns and reacts with calcium from bones and other tissues; special care should be taken when handling. Platinum was used as a cathode and a 1 cm × 1 cm square of flat silicon as the anode. Porosification exclusively took place along the anodic side of the silicon wafer. Anodization was performed with a voltage of 6 V and a current of 0.5 A for 20 min. After anodization the porous silicon was extensively rinsed in deionized (DI) H_2O and dried with nitrogen.

Micropeaked Surface. Micropeaked silicon surfaces were fabricated utilizing a modified electroless metal deposition process and chemical etching.[26,87,88] Silicon squares (1 cm × 1 cm) were chemically etched in an aqueous solution of 3.0 M HF and 14.0 mM $AgNO_3$. Etching was performed at 50 °C for 60 min. The samples were then placed in dilute nitric acid (1:9 v/v in DI H_2O) for 4 days to remove the silver coating and then dried with nitrogen.

Nanochanneled Surface. The nanochanneled surfaces were fabricated as previously described.[89] Briefly, a supporting ridge structure was etched into a 400 μm-thick, 100 mm-diameter, double side polished (100)-oriented silicon wafer and then a low stress silicon nitride layer was deposited as an etch-stop layer. A polysilicon film, acting as the base structural layer (base layer), was deposited on top of the etch-stop layer. Holes were then etched into the base layer to define the overall shape. The holes were etched through the polysilicon by chlorine plasma, with a thermally grown oxide layer used as a mask. The pore sacrificial oxide was then grown on the base layer, to determine the pore size in the final membrane. Anchor points were etched through the sacrificial oxide and the plug polysilicon was deposited to fill in the holes. The plug layer was then planarized down to the base layer, leaving the final structure with the plug layer only in the base layer openings. A protective nitride layer was then deposited on the wafer, completely covering both sides of the wafer. This layer is completely impervious to KOH chemical etch. The wafer was placed in an 80 °C KOH bath to etch. After the silicon was completely removed up to the membrane, the protective, sacrificial, and etch stop layers were removed by etching in HF.

Monocyte Isolation. Human blood was collected from three or more normal healthy individuals of varying race and age in K2 EDTA vacuette blood collection tubes (Greiner). The blood was maintained for a short period of time on ice before isolating the monocytes *via* the adherent method as outlined in Current Protocols in Immunology.[90] Briefly, the blood was diluted to twice the volume with phosphate buffer solution (PBS), and HISTOPAQUE-1077 (Sigma) was added. The gradient/blood/PBS mixture was then centrifuged at 2000 RPM for 30 min at 20 °C, with no brake. The peripheral blood mononuclear cell (PBMC) layer was isolated and washed two times with Hank's balanced salt solution (HBSS) with calcium and magnesium. The PBMC's were seeded on to T-75 culture flasks at a density of 2×10^7 cells/flask in RPMI with Glutamax (Gibco), 10% fetal bovine serum (Gibco), and 1% antibiotic/antimycotic (Sigma). The cells were placed in the incubator for 3 h, after which time, the supernatant media was aspirated off and fresh media was added. The monocytes remained attached to the surface of the flask during the aspiration process. Cells were maintained in culture for 24 h or less prior to seeding on surface.

Live/Dead Analysis. Freshly isolated monocytes were seeded on UV-treated nanomaterials surfaces at a concentration of 1×10^6 cells/mL in sterile 12- or 6-well plates. The cells were seeded at a density of 5×10^5 cells/cm^2. After 48 h the supernatant was removed for cytokine analysis and the surfaces were placed into a new well plate and stained according to manufacturer's directions. Adherent monocytes were stained with propidium iodide (Invitrogen) to indicate cell death and CellTracker Green CMFDA (5-chloromethylfluorescein diacetate; Invitrogen) to indicate live cells. The monocytes were then imaged on an Olympus BX60 fluorescent microscope. The percentage of dead cells was measured by counting the number of dead cells in 3−5 distinctive view fields on each of the three surfaces in that sampling and dividing it by the number of live cells. The area and circularity calculations were calculated by manually tracing the live fluorescent cell outline with ImageJ (National Institutes of Health; Bethesda, MD). From each of the three surface samples for that particular group, up to six cells were imaged in each of the one to three distinct views on the surface. Overall, an *n* of 3 was used for each area and circularity measurement.

Flow Cytometry. Flow cytometry was used to quantify the mean fluorescent intensity (MFI) for the reactive oxygen analyses. Cells were detached from the surface either with 0.02% EDTA in PBS[90] or 0.25% trypsin. All samples were run in through a BD FACS Calibur. The live cell population was gated to include all PMBCs.

Monocyte Identification. The isolated monocytes were stained with anti-CD-14-FITC (MY4-FITC; Beckman Coulter) as per manufacturer's directions. The percentage of monocytes was identified by excitation in the FITC emission wavelength. (Data not shown.)

Reactive Oxygen Species. To determine the optimum time point for reactive oxygen species (ROS) measurement, a time course was taken. On the basis of the cytokine analysis, two surfaces were selected for the time course, a high (micropeaked silicon), and low (tissue culture polystyrene) level immunogenic surface. These surfaces were measured for both cellular ROS and mitochondrial superoxide production at 1, 8, 16, and 24 h time points. From this set of experiments, it was determined that the maximum ROS activity occurs at the 16 h time point.

Reactive oxygen species detection is based on 5-(and-6)-carboxy-2′,7′-dichlorodihydrofluorescein diacetate (carboxy-H_2DCFDA). In the presence of ROS, carboxy- H_2DCFDA forms fluorescent carboxy-DCF. After staining the cells were detached and resuspended in PBS and fixed with 3.7% paraformaldeyde. The cells were then analyzed with flow cytometry. The intensity of the dye was characterized by the MFI and normalized to the TCPS.

Because fixed cells become permeable, imaging of live stained cells with fluorescent microscopy was performed to ensure that dye did not leach from the fixed monocytes. In this comparison, the same trends with respect to monocytes on all

surfaces were observed, concluding that dye did not leak from the permeable cells. (Data not shown.) The overall fluorescence intensity was not observed to be identical with fluorescent microscopy; however, this would be expected since flow cytometry is considered a more precise measurement tool of fluorescence.

Mitochondria are the main intercellular source of ROS. Formation of mitochondrial superoxide was detected by MitoSOX red (Invitrogen). MitoSOX red reagent is oxidized by superoxides and in doing so binds to nucleic acids in the cell and fluoresces. The cells were stained in accordance with Invitrogen's protocol. The cells were fixed with paraformaldeyde and analyzed with flow cytometry. The intensity of the dye was characterized by the mean fluorescent intensity (MFI) and normalized to the TCPS.

Cytokine and Chemokine Analysis. Luminex testing was provided by BioSource Cytokines & Signaling (Invitrogen) using a Luminex 100 instrument from Luminex Corporation (Austin, TX). For these measurements, the cytokine profile of lipopolysaccharide (LPS; Sigma; 1 μg/mL) served as a positive control to determine the maximum inflammatory response of monocytes. LPS is a major constituent of the cell wall of a gram-negative bacteria, is highly immunogenic, and is one of the best activators of monocytes/macrophages.[64] LPS was added to monocytes grown on tissue culture polystyrene to establish a positive control in which to compare the cytokine release of monocytes on the silicon surfaces. For each of the cytokine or chemokine, the supernatant from three surfaces was analyzed. The proteins to be analyzed were selected based on those significantly higher or lower in monocytes stimulated by LPS, as determined with microarray.[91] The pro-inflammatory cytokines chosen were Interleukin-one α (IL-1α), IL-1β, tumor necrosis factor α (TNF-α), interferon gamma (IFN-γ), IFN-α, IL-6 and IL-12; the anti-inflammatory cytokines: IL-6 and IL-10; and chemokines, macrophage inflammatory protein-1α and -1β (MIP-1α and MIP-1β).[63,64]

Surface Analysis and Imaging. ***Scanning Electron Microscopy: Fixing and Imaging.*** Cell morphology on different silicon surfaces was examined using SEM. The surfaces were imaged after 48 h of culture to investigate the morphology. Prior to imaging, the cells were fixed and dehydrated. The surfaces were rinsed twice in PBS and then soaked in the primary fixative of 3% glutaraldehyde (Sigma), 0.1 M of sodium cacodylate (Polysciences), and 0.1 M sucrose (Sigma, ST. Louis MO) for 72 h. The surfaces were subjected to two five-minute washes with a buffer containing 0.1 M sodium cacodylate and 0.1 M sucrose. The cells were then dehydrated by replacing the buffer with increasing concentrations of ethanol (35, 50, 70, 95, 100, and 100%) for ten minutes each. The cells were dried by replacing ethanol with hexamethyldisilazane (HMDS) (Polysciences) for 10 min. The HMDS was removed, and the surfaces were air-dried for 30 min. After mounting, the samples were coated with a 15 nm layer of gold−palladium with a sputter coater at a current of 20 mA and pressure of 0.05 mbar for 45 s. SEM imaging was conducted on the Sirion scanning electron microscope at voltages ranging from 3−5 kV.

Statistics. An average value is presented from at least three sample sets for each surface. If error bars are presented, they represent the standard error mean. For the cytokine analysis, each surface was compared with an ANOVA in each series. Single indication of significance means the p-value is less than 0.05. A double indication of significance denotes that the p-value is less than 0.01.

Acknowledgment. The authors acknowledge the following funding sources: NSF, UC Discovery Grant, the Sandler Family Foundation, and the UCSF REAC Award. All SEM was performed at the Stanford Nanocharacterization Laboratory through the Stanford CIS grant program. The nanochanneled silicon membranes were generously donated by iMEDD, Inc. Additionally we would like to thank J. Katz and her wonderful staff at the UCSF Blood Center and our blood donation volunteers: R. Thakar, E. Bachelder, A. Mendelsohn, K. Fischer, M. Steedman, and P. Ayala.

REFERENCES AND NOTES

1. Ferrara, L. A.; Fleischman, A. J.; Togawa, D.; Bauer, T. W.; Benzel, E. C.; Roy, S. An *in Vivo* Biocompatibility Assessment of Mems Materials for Spinal Fusion Monitoring. *Biomed. Microdevices* **2003**, *5*, 297–302.
2. Steeves, C. A.; Young, Y. L.; Liu, Z.; Bapat, A.; Bhalerao, K.; Soboyejo, A. B. O.; Soboyejo, W. O. Membrane Thickness Design of Implantable Bio-Mems Sensors for the *in-Situ* Monitoring of Blood Flow. *J. Mater. Sci.: Mater. Med.* **2007**, *18*, 25–37.
3. Desai, T. A.; Hansford, D.; Ferrari, M. Characterization of Micromachined Silicon Membranes for Immunoisolation and Bioseparation Applications. *J. Membr. Sci.* **1999**, *159*, 221–31.
4. Ma, B.; Liu, S.; Gan, Z. Y.; Liu, G. J.; Cai, X. X.; Zhang, H. H.; Yang, Z. G. A Pzt Insulin Pump Integrated with a Silicon Microneedle Array for Transdermal Drug Delivery. *Microfluidics and Nanofluidics* **2006**, *2*, 417–23.
5. Santini, J. T.; Cima, M. J.; Langer, R. A Controlled-Release Microchip. *Nature* **1999**, *397*, 335–8.
6. Campbell, P. K.; Jones, K. E.; Huber, R. J.; Horch, K. W.; Normann, R. A. A Silicon-Based, 3-Dimensional Neural Interface-Manufacturing Processes for an Intracortical Electrode Array. *IEEE Trans. Biomed. Eng.* **1991**, *38*, 758–68.
7. Chow, A. Y.; Pardue, M. T.; Chow, V. Y.; Peyman, G. A.; Liang, C. P.; Perlman, J. I.; Peachey, N. S. Implantation of Silicon Chip Microphotodiode Arrays into the Cat Subretinal Space. *IEEE Trans. Neural. Syst. Rehabil. Eng.* **2001**, *9*, 86–95.
8. Santiesteban, F. M. M.; Swanson, S. D.; Noll, D. C.; Anderson, D. J. Magnetic Resonance Compatibility of Multichannel Silicon Microelectrode Systems for Neural Recording and Stimulation: Design Criteria, Tests, and Recommendations. *IEEE Trans. Biomed. Eng.* **2006**, *53*, 547–58.
9. Dario, P.; Carrozza, M. C.; Benvenuto, A.; Menciassi, A. Micro-Systems in Biomedical Applications. *J. Micromech. Microeng.* **2000**, *10*, 235–44.
10. LaVan, D. A.; McGuire, T.; Langer, R. Small-Scale Systems for *in Vivo* Drug Delivery. *Nat. Biotechnol.* **2003**, *21*, 1184–91.
11. Menz, W.; Guber, A. Microstructure Technologies and Their Potential in Medical Applications. *Minim. Invasive Neurosurg.* **1994**, *37*, 21–7.
12. Mokwa, W. Medical Implants Based on Microsystems. *Meas. Sci. Technol.* **2007**, *18*, R47–R57.
13. Razzacki, S. Z.; Thwar, P. K.; Yang, M.; Ugaz, V. M.; Burns, M. A. Integrated Microsystems for Controlled Drug Delivery. *Adv. Drug Delivery Rev.* **2004**, *56*, 185–98.
14. Receveur, R. A. M.; Lindemans, F. W.; de Rooij, N. F. Microsystem Technologies for Implantable Applications. *J. Micromech. Microeng.* **2007**, *17*, R50–R80.
15. Schurr, M. O. Microsystems Technology for Medical Applications. *Minim. Invasive Ther. Allied. Technol.* **2007**, *16*, 75.
16. Staples, M.; Daniel, K.; Cima, M. J.; Langer, R. Application of Micro- and Nano-Electromechanical Devices to Drug Delivery. *Pharm. Res.* **2006**, *23*, 847–63.
17. Tao, S. L.; Desai, T. A. Microfabricated Drug Delivery Systems: From Particles to Pores. *Adv. Drug Delivery Rev.* **2003**, *55*, 315–28.
18. Wallrabe, U.; Ruther, P.; Schaller, T.; Schomburg, W. K. Microsystems in Medicine. *Int. J. Artif. Organs* **1998**, *21*, 137–46.
19. Lillis, B.; Jungk, C.; Iacopino, D.; Whelton, A.; Hurley, E.; Sheehan, M. M.; Splinter, A.; Quinn, A.; Redmond, G.; Lane, W. A. Microporous Silicon and Biosensor Development: Structural Analysis, Electrical Characterisation and Biocapacity Evaluation. *Biosens. Bioelectron.* **2005**, *21*, 282–92.
20. Park, I. Y.; Li, Z. Y.; Li, X. M.; Pisano, A. P.; Williams, R. S. Towards the Silicon Nanowire-Based Sensor for

Intracellular Biochemical Detection. *Biosens. Bioelectron.* **2007**, *22*, 2065–70.
21. De Stefano, L.; Rotiroti, L.; Rendina, I.; Moretti, L.; Scognamiglio, V.; Rossi, M.; D'Auria, S. Porous Silicon-Based Optical Microsensor for the Detection of L-Glutamine. *Biosens. Bioelectron.* **2006**, *21*, 1664–7.
22. Balarin, A.; Gamulin, O.; Ivanda, A.; Djerek, V.; Celan, O.; Music, S.; Ristic, A.; Furic, K. Structure and Optical Properties of Porous Silicon Prepared on Thin Epitaxial Silicon Layer on Silicon Substrates. *J. Mol. Struct.* **2007**, *834*, 465–70.
23. Chambon, E.; Florentin, E.; Torchynska, T.; Gonzalez-Hernandez, J.; Vorobiev, Y. Optical Properties of Porous Silicon Surface. *Microelectronics J.* **2005**, *36*, 514–7.
24. Jelinek, I.; Chvojka, T.; Vrkoslav, V.; Jindrich, J.; Lorenc, M.; Niznansky, D.; Nemec, I.; Kral, V.; Dian, J. Nanostructured Porous Silicon - Optical Properties, Surface Modification and Sensor Applications. *Chimia* **2005**, *59*, 222–5.
25. Natarajan, B.; Ramakrishnan, V.; Vasu, V.; Ramamurthy, S. Structural and Photoluminescence Properties of Porous Silicon: Effect of Hf Concentration. *Surf. Rev. Lett.* **2006**, *13*, 351–6.
26. Peng, K. Q.; Hu, J. J.; Yan, Y. J.; Wu, Y.; Fang, H.; Xu, Y.; Lee, S. T.; Zhu, J. Fabrication of Single-Crystalline Silicon Nanowires by Scratching a Silicon Surface with Catalytic Metal Particles. *Adv. Funct. Mater.* **2006**, *16*, 387–94.
27. Reddy, R. R. K.; Chadha, A.; Bhattacharya, E. Porous Silicon-Based Potentiometric Triglyceride Biosensor. *Biosens. Bioelectron.* **2001**, *16*, 313–7.
28. Wilk, S. J.; Petrossian, L.; Goryll, A.; Thorriton, T. J.; Goodnick, S. M.; Tang, J. M.; Eisenberg, R. S. Integrated Electrodes on a Silicon-Based Ion Channel Measurement Platform. *Biosens. Bioelectron.* **2007**, *23*, 183–90.
29. Chen, S. Q.; Zhu, Z. Q.; Zhu, J. Z.; Zhang, J. A.; Shi, Y. L.; Ke, Y.; Wang, W. M.; Wang, X. H.; Feng, X. A.; Luo, L. Q. Hydroxyapatite Coating on Porous Silicon Substrate Obtained by Precipitation Process. *Appl. Surf. Sci.* **2004**, *230*, 418–24.
30. Hing, K. A.; Revell, P. A.; Smith, N.; Buckland, T. Effect of Silicon Level on Rate, Quality and Progression of Bone Healing within Silicate-Substituted Porous Hydroxyapatite Scaffolds. *Biomaterials* **2006**, *27*, 5014–26.
31. Weis, R. P.; Montchamp, J. L.; Coffer, J. L.; Attiah, D. G.; Desai, T. A. Calcified Nanostructured Silicon Wafer Surfaces for Biosensing: Effects of Surface Modification on Bioactivity. *Dis. Markers* **2002**, *18*, 159–65.
32. Edquist, B. T.; White, T. B.; Fulmer, G. R.; Thornberry, D. R.; Porter, L. A. Degradation of Long-Chain Alkyl Functionalized Porous Silicon in Simulated Acellular Plasma. *Abstr. Papers Am. Chem. Soc.* **2006**, *231*, 292-CHED
33. Fulmer, G. R.; Thornberry, D. R.; Rhodes, S. D.; Porter, L. A. Degradation of Functionalized Porous Silicon in Simulated Body Fluid. *Abstr. Papers Am. Chem. Soc.* **2005**, *229*, U514.
34. Thornberry, D. R.; Fulmer, G. R.; Rhodes, S. D.; Porter, L. A. Degradation of Functionalized Porous Silicon in Simulated Blood, Gastric, and Intestinal Fluids. *Abstr. Papers Am. Chem. Soc.* **2005**, *229*, U679.
35. Thornberry, D. R.; Fulmer, G. R.; Rhodes, S. D.; Porter, L. A. Degradation of Functionalized Porous Silicon in Simulated Gastric Fluid. *Abstr. Papers Am. Chem. Soc.* **2005**, *229*, U514.
36. White, T. B.; Edquist, B. T.; Fulmer, G. R.; Thornberry, D. R.; Porter, L. A. Degradation of Short-Chain Alkyl Functionalized Porous Silicon in Simulated Acellular Plasma. *Abstr. Papers Am. Chem. Soc.* **2006**, 231.
37. Kulkarni, S. S.; Orth, R.; Ferrari, M.; Moldovan, N. I. Micropatterning of Endothelial Cells by Guided Stimulation with Angiogenic Factors. *Biosens. Bioelectron.* **2004**, *19*, 1401–7.
38. Coffer, J. L.; Whitehead, M. A.; Nagesha, D. K.; Mukherjee, P.; Akkaraju, G.; Totolici, M.; Saffie, R. S.; Canham, L. T. Porous Silicon-Based Scaffolds for Tissue Engineering and Other Biomedical Applications. *Phys. Status Solidi A* **2005**, *202*, 1451–5.
39. Low, S. P.; Williams, K. A.; Canham, L. T.; Voelcker, N. H. Evaluation of Mammalian Cell Adhesion on Surface-Modified Porous Silicon. *Biomaterials* **2006**, *27*, 4538–46.
40. Balasundaram, G.; Webster, T. J. Increased Osteoblast Adhesion on Nanograined Ti Modified with Krsr. *J. Biomed. Mater. Res.* **2007**, *80A*, 602–11.
41. Lopez, C. A.; Fleischman, A. J.; Roy, S.; Desai, T. A. Evaluation of Silicon Nanoporous Membranes and Ecm-Based Micro Environments on Neurosecretory Cells. *Biomaterials* **2006**, *27*, 3075–83.
42. Popat, K. C.; Daniels, R. H.; Dubrow, R. S.; Hardev, V.; Desai, T. A. Nanostructured Surfaces for Bone Biotemplating Applications. *J. Orthop. Res.* **2006**, *24*, 619–27.
43. Coffer, J. L.; Montchamp, J. L.; Aimone, J. B.; Weis, R. P. Routes to Calcified Porous Silicon: Implications for Drug Delivery and Biosensing. *Phys. Status Solidi A* **2003**, *197*, 336–39.
44. Foraker, A. B.; Walczak, R. J.; Cohen, M. H.; Boiarski, T. A.; Grove, C. F.; Swaan, P. W. Microfabricated Porous Silicon Particles Enhance Paracellular Delivery of Insulin across Intestinal Caco-2 Cell Monolayers. *Pharm. Res.* **2003**, *20*, 110–6.
45. Sakamoto, J. H.; Smith, B. R.; Xie, B.; Rokhlin, S. I.; Lee, S. C.; Ferrari, M. The Molecular Analysis of Breast Cancer Utilizing Targeted Nanoparticle Based Ultrasound Contrast Agents. *Technol. Cancer. Res. Treat.* **2005**, *4*, 627–36.
46. Salonen, J.; Laitinen, L.; Kaukonen, A. M.; Tuura, J.; Bjorkqvist, M.; Heikkila, T.; Vaha-Heikkila, K.; Hirvonen, J.; Lehto, V. P. Mesoporous Silicon Microparticles for Oral Drug Delivery: Loading and Release of Five Model Drugs. *J. Controlled Release* **2005**, *108*, 362–74.
47. Desai, T. A.; Chu, W. H.; Tu, J. K.; Beattie, G. M.; Hayek, A.; Ferrari, M. Microfabricated Immunoisolating Biocapsules. *Biotechnol. Bioeng.* **1998**, *57*, 118–20.
48. Edell, D. J.; Toi, V. V.; McNeil, V. M.; Clark, L. D. Factors Influencing the Biocompatibility of Insertable Silicon Microshafts in Cerebral Cortex. *IEEE Trans. Biomed. Eng.* **1992**, *39*, 635–43.
49. Kotzar, G.; Freas, M.; Abel, P.; Fleischman, A.; Roy, S.; Zorman, C.; Moran, J. M.; Melzak, J. Evaluation of Mems Materials of Construction for Implantable Medical Devices. *Biomaterials* **2002**, *23*, 2737–50.
50. Voskerician, G.; Shive, M. S.; Shawgo, R. S.; von Recum, H.; Anderson, J. M.; Cima, M. J.; Langer, R. Biocompatibility and Biofouling of Mems Drug Delivery Devices. *Biomaterials* **2003**, *24*, 1959–67.
51. Lan, S.; Veiseh, M.; Zhang, M. Q. Surface Modification of Silicon and Gold-Patterned Silicon Surfaces for Improved Biocompatibility and Cell Patterning Selectivity. *Biosens. Bioelectron.* **2005**, *20*, 1697–708.
52. Bayliss, S. C.; Buckberry, L. D.; Fletcher, I.; Tobin, M. J. The Culture of Neurons on Silicon. *Sens. Actuators, A* **1999**, *74*, 139–42.
53. Bayliss, S. C.; Harris, P. J.; Buckberry, L. D.; Rousseau, C. Phosphate and Cell Growth on Nanostructured Semiconductors. *J. Mater. Sci. Lett.* **1997**, *16*, 737–40.
54. Canham, L. T. In *Porous Silicon as a Therapeutic Material*, Proceedings of theAnnual International IEEE-EMBS Special Topic Conference on Microtechnologies in Medicine & Biology, Lyon, France, 2000; IEEE: Lyon, France, 2000; pp 109−12..
55. Chin, V.; Collins, B. E.; Sailor, M. J.; Bhatia, S. N. Compatibility of Primary Hepatocytes with Oxidized Nanoporous Silicon. *Adv. Mater. (Weinheim, Ger.)* **2001**, *13*, 1877+
56. Craighead, H. G.; James, C. D.; Turner, A. M. P. Chemical and Topographical Patterning for Directed Cell Attachment. *Curr. Opin. Solid State Mater. Sci.* **2001**, *5*, 177–84.
57. Rosengren, A.; Wallman, L.; Danielsen, N.; Laurell, T.; Bjursten, L. M. Tissue Reactions Evoked by Porous and Plane Surfaces Made out of Silicon and Titanium. *IEEE Trans. Biomed. Eng.* **2002**, *49*, 392–99.

58. Serrano, M. C.; Pagani, R.; Vallet-Regi, M.; Pena, J.; Ramila, A.; Izquierdo, I.; Portoles, M. T. *In Vitro* Biocompatibility Assessment of Poly(Epsilon-Caprolactone) Films Using L929 Mouse Fibroblasts. *Biomaterials* **2004**, *25*, 5603–11.
59. Anderson, J. M.; Defife, K.; McNally, A.; Collier, T.; Jenney, C. Monocyte, Macrophage and Foreign Body Giant Cell Interactions with Molecularly Engineered Surfaces. *J. Mater. Sci. Mater. Med.* **1999**, *10*, 579–88.
60. Jenney, C. R.; DeFife, K. M.; Colton, E.; Anderson, J. M. Human Monocyte/Macrophage Adhesion, Macrophage Motility, and Il-4-Induced Foreign Body Giant Cell Formation on Silane-Modified Surfaces *in Vitro*. Student Research Award in the Master's Degree Candidate Category, 24th Annual Meeting of the Society for Biomaterials, San Diego, Ca, April 22−26, 1998. *J. Biomed. Mater. Res.* **1998**, *41A*, 171–84.
61. Lollini, P. L.; De Giovanni, C.; Pannellini, T.; Cavallo, F.; Forni, G.; Nanni, P. Cancer Immunoprevention. *Future Oncol.* **2005**, *1*, 57–66.
62. Bode, J. G.; Nimmesgern, A.; Schmitz, J.; Schaper, F.; Schmitt, M.; Frisch, W.; Haussinger, D.; Heinrich, P. C.; Graeve, L. Lps and Tnfalpha Induce Socs3 Mrna and Inhibit Il-6-Induced Activation of Stat3 in Macrophages. *FEBS Lett.* **1999**, *463*, 365–70.
63. Janeway, C.; Travers, P.; Walport, M.; Shlomchik, M., *Immunobiology*, 5th ed.; Garland Science: New York, 2001.
64. Paul, W. E., *Fundamental Immunology*, 4th ed.; Raven Press: New York, 1994.
65. Tournier, J. N.; Jouan, A.; Mathieu, J.; Drouet, E. Gulf War Syndrome: Could It Be Triggered by Biological Warfare-Vaccines Using Pertussis as an Adjuvant. *Med. Hypotheses* **2002**, *58*, 291–92.
66. Padera, R. F.; Colton, C. K. Time Course of Membrane Microarchitecture-Driven Neovascularization. *Biomaterials* **1996**, *17*, 277–84.
67. Bayliss, S. C.; Buckberry, L. D.; Harris, P. J.; Tobin, M. Nature of the Silicon-Animal Cell Interface. *J. Porous Mater.* **2000**, *7*, 191–195.
68. Magazine, H. I.; Liu, Y.; Bilfinger, T. V.; Fricchione, G. L.; Stefano, G. B. Morphine-Induced Conformational Changes in Human Monocytes, Granulocytes, and Endothelial Cells and in Invertebrate Immunocytes and Microglia Are Mediated by Nitric Oxide. *J. Immunol.* **1996**, *156*, 4845–50.
69. Thomsen, P.; Gretzer, C. Macrophage Interactions with Modified Material Surfaces. *Curr. Opin. Solid State Mater. Sci.* **2001**, *5*, 163–176.
70. Suska, F.; Gretzer, C.; Esposito, M.; Tengvall, P.; Thomsen, P. Monocyte Viability on Titanium and Copper Coated Titanium. *Biomaterials* **2005**, *26*, 5942–50.
71. Bruegel, M.; Teupser, D.; Haffner, I.; Mueller, M.; Thiery, J. Statins Reduce Macrophage Inflammatory Protein-1alpha Expression in Human Activated Monocytes. *Clin. Exp. Pharmacol. Physiol.* **2006**, *33*, 1144–9.
72. Nel, A.; Xia, T.; Madler, L.; Li, N. Toxic Potential of Materials at the Nanolevel. *Science* **2006**, *311*, 622–27.
73. Seal, S.; Krezoski, S.; Barr, T. L.; Petering, D. H.; Klinowski, J.; Evans, P. H. Surface Chemistry and Biological Pathogenicity of Silicates: An X-Ray Photoelectron Spectroscopic Study. *Proc. Biol. Sci.* **1996**, *263*, 943–51.
74. Epstein, E. Silicon. *Annu. Rev. Plant Physiol. Plant Mol. Biol.* **1999**, *50*, 641–64.
75. Zhou, S.; Liao, X.; Li, X.; Deng, X.; Li, H. Poly-D,L-Lactide-Co-Poly(Ethylene Glycol) Microspheres as Potential Vaccine Delivery Systems. *J. Controlled Release* **2003**, *86*, 195–205.
76. Mayne, A. H.; Bayliss, S. C.; Barr, P.; Tobin, M.; Buckberry, L. D. Biologically Interfaced Porous Silicon Devices. *Phys. Status Solidi A* **2000**, *182*, 505–513.
77. Mizutani, H. Studies on the Cytotoxicity of Silver Alloys Be Means of Cell Culture (Author's Transl). *Shika Rikogaku Zasshi* **1976**, *17*, 145–61.
78. Sompayrac, L. *How the Immune System Works*. Blackwell Publishing Limited: New York, 2002.
79. Ainslie, K. M.; Bachelder, E. M.; Borkar, S.; Zahr, A. S.; Sen, A.; Badding, J. V.; Pishko, M. V. Cell Adhesion on Nanofibrous Polytetrafluoroethylene (Nptfe). *Langmuir* **2007**, *23*, 747–54.
80. Xia, T.; Kovochich, M.; Brant, J.; Hotze, M.; Sempf, J.; Oberley, T.; Sioutas, C.; Yeh, J. I.; Wiesner, M. R.; Nel, A. E. Comparison of the Abilities of Ambient and Manufactured Nanoparticles to Induce Cellular Toxicity According to an Oxidative Stress Paradigm. *Nano Lett.* **2006**, *6*, 1794–807.
81. Matzinger, P. The Danger Model: A Renewed Sense of Self. *Science* **2002**, *296*, 301–5.
82. Abramov, A. Y.; Scorziello, A.; Duchen, M. R. Three Distinct Mechanisms Generate Oxygen Free Radicals in Neurons and Contribute to Cell Death During Anoxia and Reoxygenation. *J. Neurosci.* **2007**, *27*, 1129–38.
83. Batandier, C.; Fontaine, E.; Keriel, C.; Leverve, X. M. Determination of Mitochondrial Reactive Oxygen Species: Methodological Aspects. *J. Cell. Mol. Med.* **2002**, *6*, 175–87.
84. Ainslie, K. M.; Sharma, G.; Dyer, M. A.; Grimes, C. A.; Pishko, M. V. Attenuation of Protein Adsorption on Static and Oscillating Magnetostrictive Nanowires. *Nano Lett.* **2005**, *5*, 1852–1856.
85. Wisniewski, N.; Reichert, M. Methods for Reducing Biosensor Membrane Biofouling. *Colloids and Surfaces B: Biointerfaces* **2000**, *18*, 197–219.
86. Foraker, A. B.; Walczak, R. J.; Cohen, M. H.; Boiarski, T. A.; Grove, C. F.; Swaan, P. W. Microfabricated Porous Silicon Particles Enhance Paracellular Delivery of Insulin across Intestinal Caco-2 Cell Monolayers. *Pharm. Res.* **2003**, *20*, 110–6.
87. Peng, K. Q.; Yan, Y. J.; Gao, S. P.; Zhu, J. Synthesis of Large-Area Silicon Nanowire Arrays *via* Self-Assembling Nanoelectrochemistry. *Adv. Mater. (Weinheim, Ger.)* **2002**, *14*, 1164–1167.
88. Peng, K. Q.; Yan, Y. J.; Gao, S. P.; Zhu, J. Dendrite-Assisted Growth of Silicon Nanowires in Electroless Metal Deposition. *Adv. Funct. Mater.* **2003**, *13*, 127–132.
89. Martin, F.; Walczak, R.; Boiarski, A.; Cohen, M.; West, T.; Cosentino, C.; Shapiro, J.; Ferrari, M. Tailoring Width of Microfabricated Nanochannels to Solute Size Can Be Used to Control Diffusion Kinetics. *J. Controlled Release* **2005**, *102*, 123–33.
90. Coligan, J. E.; Kruisbeek, A. M.; Margulies, D. H.; Shevach, E. M.; Strober, W. *Current Protocols in Immunology*; John Wiley & Sons, Inc.: New York, 2005; Vol. 1, p 7.6A.
91. Suzuki, T.; Hashimoto, S.; Toyoda, N.; Nagai, S.; Yamazaki, N.; Dong, H. Y.; Sakai, J.; Yamashita, T.; Nukiwa, T.; Matsushima, K. Comprehensive Gene Expression Profile of Lps-Stimulated Human Monocytes by Sage. *Blood* **2000**, *96*, 2584–91.